DOI: 10.1002/ejic.201100394

Influence of Hydrogen Bonding on the Hysteresis Width in Iron(II) Spin-Crossover Complexes

Birgit Weber,*[a,b] Wolfgang Bauer,[b] Toni Pfaffeneder,[b] Marinela M. Dîrtu,[c] Anil D. Naik,[c] Aurelian Rotaru,[d] and Yann Garcia*[c]

Keywords: Molecular bistability / Spin crossover / Memory effect / Hydrogen bonds / Crystal engineering

A detailed investigation on the properties of the high-temperature and low-temperature modifications of the iron(II) spin-crossover complex [FeL1(HIm)$_2$] (**1**) and its isotopic deuterium-labelled analogue [FeL1(DIm)$_2$] (**1**D), and the pair [FeL2(azpy)]·MeOH/[FeL2(azpy)]·CD_3OD/[FeL2(azpy)] (**2**·MeOH/**2**·CD_3OD/**2**), in which L1 and L2 are tetradentate $N_2O_2^{2-}$-coordinating Schiff base like ligands, L1 = {diethyl (*E*,*E*)-2,2′-[1,2-phenylbis(iminomethylidyne)]bis[3-oxobutanoate](2–)-*N*,*N*′,O^3,$O^{3'}$}, L2 = {2,2′-[1,2-phenylbis(iminomethylidyne)]bis[1-phenylbutane-1,3-dione](2–)-*N*,*N*′,O^3,$O^{3'}$}, HIm = imidazole, and azpy = 4,4′-azopyridine, is presented. All complexes except **2** show a cooperative spin transition with hysteresis widths between approximately 5 K (**1**^{LT} and **1**^{LT}D), 70 K (**1**^{HT}[9] and **1**^{HT}D, around room temperature), and 80 K (**2**·MeOH and **2**·CD_3OD). In all cases, an influence of the H/D exchange on the transition temperature and the hysteresis width is observed. For **1**^{HT}, first-order reversal curves (FORCs) have been recorded, and a statistical analysis gives the interaction parameter J = 560 K, indicating strong intermolecular interactions. X-ray structural analysis of the different samples (**1**^{HT}[9] and **1**^{HT}D: HS; **1**^{LT} and **1**^{LT}D: LS; and **2**·MeOH and **2**·CD_3OD: HS) gives a deeper insight into the molecular packing in the crystals and helps explain the increase of cooperative interactions during the spin transition. In all cases, one hydrogen bond involves an oxygen atom of the Schiff base like ligand that serves as a donor for the iron centre. The influence of this hydrogen bond on the ligand field strength of the iron centre is discussed and a new model is developed to explain the observed connection between hydrogen bonds and exceptionally wide hysteresis loops for the complexes presented in this work and other examples from the literature.

Introduction

There is an ongoing interest in the bistability of spin-crossover (SCO) compounds[1] as the thermochromism associated with the spin transition (ST) makes them potentially useful for various applications, such as display and memory device units,[2] sensors[3] and cold channel control units in food and medical storage devices.[4] Recent research activities in this field explore the possibility of combining the SCO bistability with additional properties (e.g., liquid crystalline properties[5] and magnetic exchange interactions[6]) resulting in multifunctional SCO materials,[7] or are focused on the rational design of nano-structured SCO materials and their chemical and physical properties.[8] Of the possible types of ST (gradual, abrupt, with hysteresis, stepwise, incomplete), much of the interest is focused on the bistability in highly cooperative systems (hysteresis or memory effect) as such compounds can exist in two different electronic states depending on the history of the system. In this regard, we recently characterised an iron(II) SCO complex with a 70 K wide thermal hysteresis loop around room temperature based on a 2D network of hydrogen bonds between the complex molecules {compound **1**-[FeL1(HIm)$_2$]}.[9] The possibility to influence the ST behaviour by hydrogen bonds has been already introduced in the literature. Several examples demonstrate an influence of the presence or absence of hydrogen bonds on both the transition temperature[10–13] as well as on cooperative effects.[9,13–15] For some of the examples, an influence of the hydrogen bonds on the electron density of donor atoms and by this on the ligand field strength is discussed.[10–13] To date, however, no consistent model for the explanation of the different effects is available. A detailed understanding of the interplay of hydrogen bonds and wide hysteresis loops is essential for a purposeful synthesis of SCO materials for potential applications.

We decided to use two different approaches to more clearly investigate the effect of hydrogen bonds on the coop-

[a] Inorganic Chemistry II, Universität Bayreuth
Universitätsstraße 30, NW I, 95440 Bayreuth, Germany
Fax: +49-921-552157
E-mail: weber@uni-bayreuth.de
[b] Center for Integrated Protein Science Munich at the Department of Chemistry and Biochemistry, Ludwig-Maximilians-Universität München
Butenandtstr. 5-13 (Haus F), 81377 München, Germany
[c] Institute of Condensed Matter and Nanosciences, Université Catholique de Louvain
Place L. Pasteur, 1, 1348 Louvain-la-Neuve, Belgium
E-mail: Yann.Garcia@uclouvain.be
[d] Department of Electrical Engineering and Computer Science, "Stefan cel Mare" University
University Street, No. 13, Suceava 720229, Romania

erative interactions and the transition temperature of our systems. From one side we are searching for more examples of complexes with wide hysteresis loops and hydrogen bonds. Here, we obtained a 1D chain iron(II) SCO complex with an 80 K-wide hysteresis loop, probably also due to the presence of hydrogen bonds (compound **2**·MeOH). For this complex, a second modification with a gradual SCO behaviour was obtained (compound **2**). Additionally, we decided to investigate complexes **1** and **2**·MeOH with all hydrogen atoms involved in the hydrogen-bond network substituted by deuterium. This information, together with data detailing a second modification of compound **1** with a 4 K wide hysteresis loop reported by Müller et al.[16] and the variety of other literature examples, build the foundation for a model to explain the different effects, which are presented in this work.

In Scheme 1, the ligands used to modify **1** (H_2L1 and HIm) and **2** (H_2L2 and azpy) are given (L1 = {diethyl (*E*,*E*)-2,2′-[1,2-phenylbis(iminomethylidyne)]bis[3-oxobutanoate]-(2–)-*N*,*N*′,O^3,$O^{3'}$}, L2 = {2,2′-[1,2-phenylbis(iminomethylidyne)]bis[1-phenylbutane-1,3-dione](2–)-*N*,*N*′,O^3,$O^{3'}$}, HIm = imidazole and azpy = 4,4′-azopyridine).

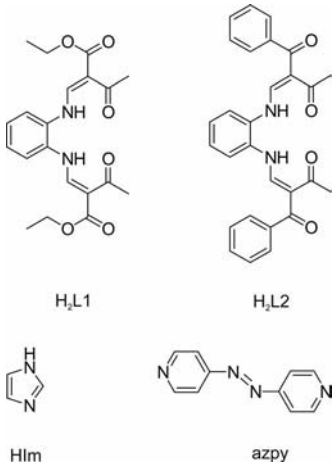

Scheme 1. Schematic representation of the equatorial ligands H_2L1 and H_2L2 and the axial ligands imidazole (HIm) and 4,4′-azopyridine (azpy).

Results

Synthesis and General Characterisation

The reaction of [FeL1(MeOH)$_2$] with an excess of imidazole in methanol leads to two different modifications of the corresponding imidazole diadduct [FeL1(HIm)$_2$] (**1**) as given in Scheme 2. Whereas for the modification with the 70 K wide thermal hysteresis around room temperature, an exact 1:2 ratio of FeL1/HIm is obtained as confirmed by X-ray structural and elemental analyses, for the second modification the exact composition is unclear. According to literature, the formula is [FeL1(HIm)$_x$] with values of x between 1.8 and 2.2.[16] In both cases, a 4 K wide thermal hysteresis loop above room temperature is observed. Although the loss of cooperative interactions when going from the exact 1:2 ratio to a higher or lower imidazole content can easily be explained by the partial destruction of the hydrogen-bond network responsible for the cooperative interactions, it is puzzling that the same transition curve is obtained irrespective of the FeL1/HIm ratio. We therefore decided to have a deeper look into this matter before starting any experiments with deuteriated imidazole.

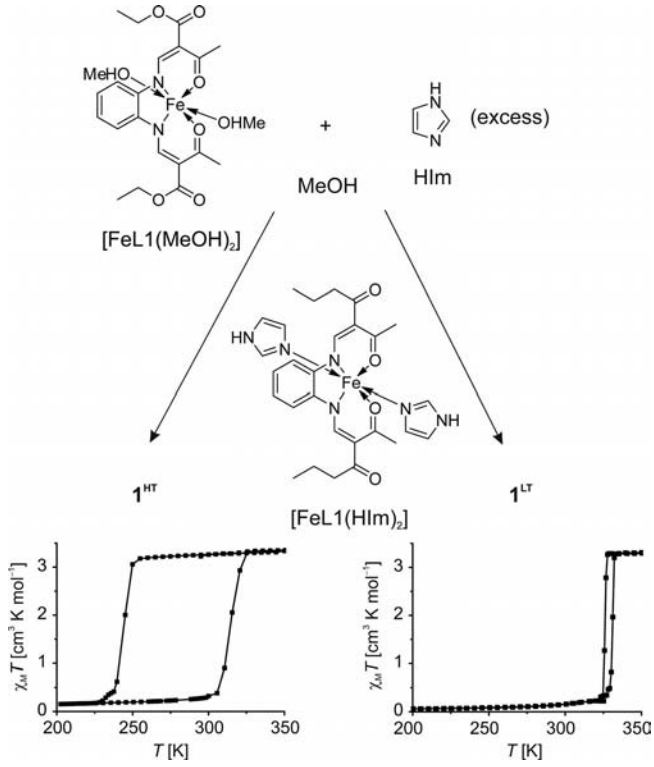

Scheme 2. Synthetic approach towards the two different modifications of the complex [FeL1(HIm)$_2$].

The results of different synthetic approaches are summarised in Scheme 2. For the modification resulting in the wide thermal hysteresis loop, a higher ratio of FeL1/HIm was necessary (1:50 instead of 1:30) and significantly less solvent was used (18 mL of MeOH instead of 67 mL per mmol of iron complex). In contrast to literature results, however, the obtained precipitate of the second modification has exactly the same composition (FeL1/HIm = 1:2) as the modification with wide thermal hysteresis loop. Differences were observed when different times were allowed for precipitation to occur. The compound with the wide hysteresis loop precipitates from boiling solution (high-temperature modification, $\mathbf{1}^{HT}$), whereas the solution with the lower concentration is clear and the precipitate is obtained after standing for a period at room temperature (fine needles) or at 4 °C (powder, low temperature modification, $\mathbf{1}^{LT}$). The magnetic properties of the powder and the fine crystalline sample of $\mathbf{1}^{LT}$ are identical. Another possibility to obtain $\mathbf{1}^{LT}$ is to store the filtrate of the reaction mixture of $\mathbf{1}^{HT}$ at 4 °C.

The powder sample of **2** can be obtained by the direct conversion of [FeL2(MeOH)$_2$] and azopyridine in methanol. Single crystals of **2**·MeOH and **2**·CD_3OD were obtained by slow diffusion techniques. Heating the crystals above room temperature leads to a loss of the included methanol and **2** is obtained. To prevent the loss of the solvent, the crystals are stored at 4 °C.

Magnetic Measurements

In Figure 1, the ST curves of $\mathbf{1}^{HT}$ and $\mathbf{1}^{LT}$ are compared with those obtained for the analogous complexes with [D_4]-imidazole, $\mathbf{1}^{HT}$D and $\mathbf{1}^{LT}$D. For the complex $\mathbf{1}^{LT}$, slightly different transition temperatures are obtained compared with the results described by Müller et al.[16] At room temperature, the $\chi_M T$ product is with 0.15 $cm^3 mol^{-1} K$ in the region typical for an iron(II) complex in the low-spin (LS) state. Upon heating, the magnetic moment remains constant up to 328 K, after which an abrupt transition in the HS state takes place with a transition temperature (HS molar fraction; γ_{HS} = 0.5) of $T_{1/2}{}^{\uparrow}$ = 331 K. At 345 K, the $\chi_M T$ product is with 3.29 $cm^3 mol^{-1} K$ in the region typical for an iron(II) complex in the HS state. Upon cooling, the magnetic moment remains constant down to 328 K. Below this temperature an abrupt transition in the LS state takes place with $T_{1/2}{}^{\downarrow}$ = 326 K. Upon deuteriation, the transition temperature in the heating mode is shifted by 1 K to higher temperature, whereas the transition temperature in the cooling mode remains the same ($T_{1/2}{}^{\uparrow}$ = 332 K and $T_{1/2}{}^{\downarrow}$ = 326 K for $\mathbf{1}^{LT}$D). The width of the thermal hysteresis loop increases from 5 to 6 K. The measurements were reproduced twice (for all samples) to verify the observed trend.

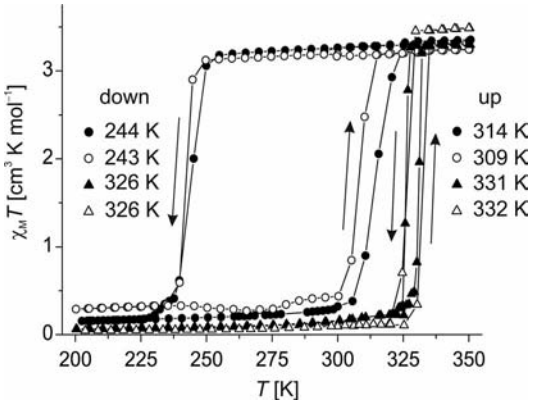

Figure 1. Thermal variation of the $\chi_M T$ product of the different modifications of **1** discussed in this work: wide hysteresis of $\mathbf{1}^{HT}$ (circles) and $\mathbf{1}^{HT}$D (open circles) and small hysteresis of $\mathbf{1}^{LT}$ (triangles) and $\mathbf{1}^{LT}$D (open triangles).

The transition curves of $\mathbf{1}^{HT}$ and $\mathbf{1}^{HT}$D are very similar, and a pronounced difference is only obtained for the transition temperature in the heating mode that is with a value of 309 K in the deuteriated compound, 5 K lower than the original complex. In the cooling mode, the transition temperature is also shifted towards lower temperatures, but only by 1 K (243 instead of 244 K). As a consequence, the width of the thermal hysteresis loop is reduced by 4 K (from 70 to 66 K) upon H/D exchange. This significant change in the width of the hysteresis loop upon deuteriation for both samples clearly demonstrates that the hydrogen-bond network influences the hysteresis width in this complex.

In Figure 2, the ST curves of **2**·MeOH, **2**·CD_3OD and the solvent-free samples of **2** are displayed. The shape of the curve progression is very similar for the two solvated compounds. For the first cycle, the magnetic behaviour was measured in the 50–280 K temperature range. After heating to 300 K, significant changes in the ST behaviour were observed, resulting in a decrease in the hysteresis loop width and the overall completeness of the SCO. Measurements up to 400 K cause a complete loss of the solvent methanol, and the ST is shifted to a higher temperature, its curve progression becoming gradual (**2**·MeOH: $T_{1/2}$ = 314 K; **2**·CD_3OD: $T_{1/2}$ = 310 K). The same gradual curve progression is obtained for a separately prepared powder sample of **2**. Thermogravimetric measurements of **2**·MeOH and **2**·CD_3OD confirm the presumption that the loss of one methanol molecule has to be responsible for the different spin transition behaviour. At 280 K, the $\chi_M T$ product of **2**·MeOH is with 3.41 $cm^3 mol^{-1} K$ in the typical range expected for an iron(II) HS centre, as for the $\chi_M T$ value of

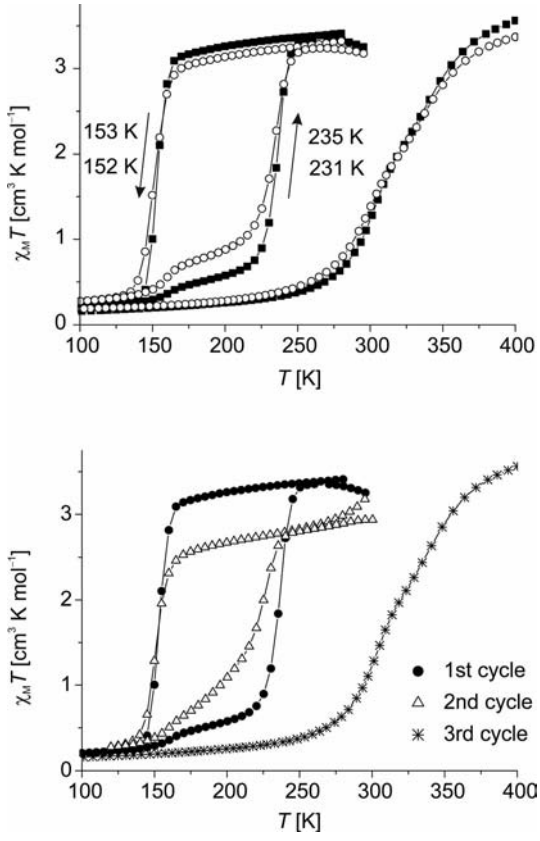

Figure 2. Top: Thermal variation of the $\chi_M T$ product of the complexes **2**·MeOH (squares) and **2**·CD_3OD (open circles). Comparison of the hysteresis loop of **2**·MeOH and **2**·CD_3OD and the gradual spin transition after tempering to 400 K. Bottom: Thermal variation of the $\chi_M T$ product of the complexes **2**·CD_3OD at the first cycle (circles), second cycle (after heating to 300 K, open triangles) and after heating to 400 K (stars).

2·CD_3OD with 3.32 $cm^3 mol^{-1} K$. Upon cooling, the $\chi_M T$ values of **2**·MeOH remain approximately constant between 280 and 164 K. Over the range 164–130 K an abrupt ST takes place to a minimum value of 0.28 $cm^3 mol^{-1} K$, indicating that all the iron(II) sites are in the LS state. Below 130 K, the $\chi_M T$ values remain approximately constant again. The $T_{1/2}$ value of this SCO is 153 K. The $\chi_M T$ values of **2**·CD_3OD remain approximately constant between 280 and 169 K, then over the range 169–125 K the $\chi_M T$ values rapidly decrease to attain a minimum value of 0.32 $cm^3 mol^{-1} K$. Below 125 K, the $\chi_M T$ values remain approximately constant. The $T_{1/2}$ value of this SCO is 152 K. For both compounds, thermal hysteresis is observed in the $\chi_M T$ values upon heating. Above 144 K, the $\chi_M T$ values of **2**·MeOH increase gradually, then, above 200 K, rapidly, to attain a maximum value of 3.65 $cm^3 mol^{-1} K$ at 265 K, indicative of HS iron(II). The $T_{1/2}$ value of this step is 235 K. The $\chi_M T$ values of **2**·CD_3OD increase, first gradually above 140 K, then rapidly above 200 K, to attain a maximum value of 3.23 $cm^3 mol^{-1} K$ at 260 K. The $T_{1/2}$ value of this SCO is 231 K. This means a thermal hysteresis loop of 82 K for **2**·MeOH and 79 K for **2**·CD_3OD. The small step in the heating mode is probably an indication for a partial loss of the included methanol molecules.

FORC Analysis

To obtain a complete picture of the interaction distribution in $\mathbf{1}^{HT}$, a set of first order reversal curves (FORCs) have been recorded (Figure 3). For each reversal temperature, $T_a = [T_{HS}, T_{LS}]$ (T_{HS} and T_{LS} are the temperatures for which the system is saturated in the HS state and in the LS state, respectively), by steps of 0.5 K, the magnetisation is recorded for decreasing temperatures T_b spanning from T_a to T_{LS} also in steps of 0.5 K. The full set of FORCs is then transformed into the so-called FORC distribution defined by Equation (1) by using the original algorithm developed by Pike.[17]

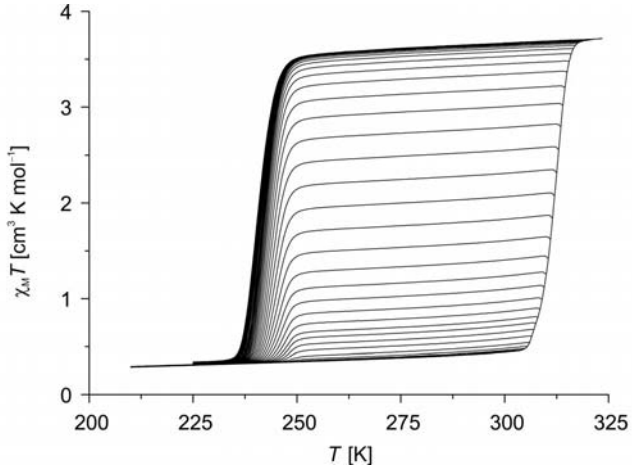

Figure 3. FORCs of the thermal hysteresis loop of $\mathbf{1}^{HT}$ recorded in the cooling mode.

$$\rho(T_a, T_b) = -\frac{\partial^2 n_{HS}(T_a, T_b)}{\partial T_a \partial T_b} \quad (1)$$

Finally, the set of the variables is changed from T_a, T_b to "coercivity" (c) and "bias" (b), as indicated in Equations (2) and (3).

$$c = \frac{T_a - T_b}{2}, \quad (2)$$

$$b = \frac{T_a + T_b}{2}, \quad (3)$$

The "bias" parameter, which is related to the equilibrium temperature $T_{1/2}$, roughly corresponds to the energy gap Δ between the HS and LS states. The "coercivity", which is related to the hysteresis width, reflects the strength of intradomain interactions, which is characterised by the J parameter.[18,19] J corresponds to an interaction parameter derived from a two-level Ising-like description of interacting SCO units (Figure 4).

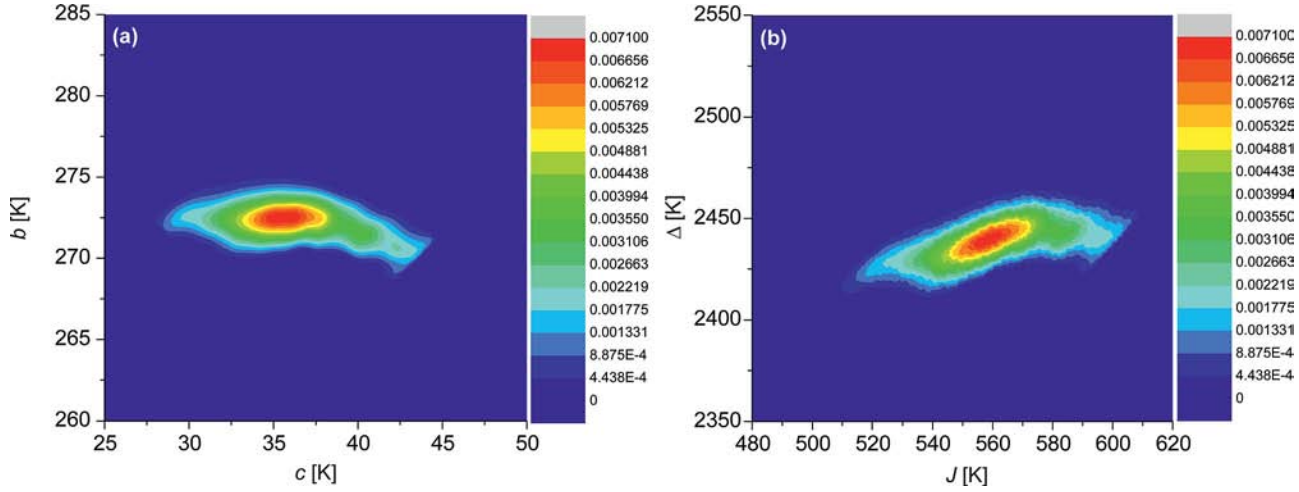

Figure 4. Experimental FORC diagram derived from Figure 3, in: (a) coercivity-bias coordinates and (b) in J-Δ coordinates. Probability that a single domain is characterised by a given value is given by its shade (very low in the blue region and very high in the red region).

Further, we discuss the FORC data in terms of the standard deviations σ and of the dimensionless correlation parameter $r_{b,c}$ defined in Equation (4).

$$r_{b,c} = \mathrm{cov}(b,c)/\sigma(b)\sigma(c) \quad (4)$$

The main parameters obtained from statistical analysis of the FORC diagrams are collected in Table 1.

Table 1. Statistical analysis of the FORC distributions obtained on $\mathbf{1}^{HT}$.

$\bar{b}$[a] [K]	$\bar{c}$[a] [K]	$\sigma(b)$ [K]	$\sigma(c)$ [K]	$r_{c,b}$ [K]	$\bar{J}$[a] [K]	$\sigma(J)$ [K]	$\bar{\Delta}$[a] [K]	$\sigma(\Delta)$ [K]	$r_{J,\Delta}$ [K]
272.2	36.1	1.1	3.4	–0.31	560	20.3	2439	11.3	0.59

[a] $\bar{b}$, $\bar{c}$, $\bar{J}$, $\bar{\Delta}$, represent the mean values of the parameters b, c, Δ and J, respectively.

The mean value of the interaction parameter, J = 560 K and an energy gap Δ = 2439 K have been determined for $\mathbf{1}^{HT}$. This interaction parameter is much higher than that of the model 2D ST coordination polymer $[Fe(btr)_2(NCS)_2]\cdot H_2O$ (J = 235 K),[19] which presents a hysteresis width of 25 K,[20] free of any structural phase transition.[21] It is also higher than that of the 1D ST chain compound $[Fe(NH_2trz)_3](NO_3)_2$ (J = 496 K), which present a hysteresis width of 33 K and which is also free of structural phase transformation.[22] A strong correlation between statistical parameters is observed, which suggests that the intralayer interaction strength within the 2D hydrogen-bond network[9] is higher than the interlayer interaction thus giving rise to anisotropy in the propagation of the interactions, that is, along the 2D layer of $\mathbf{1}^{HT}$. This result agrees very well with earlier FORCs studies carried out on 1D ST systems that concluded on the nature of the correlation taking its origin from an anisotropy source induced, for instance, by interchain interactions[22] or by an external pressure.[23] The composition distribution suggested by Tanasa et al.[19] in a diluted 2D ST system as the origin of the correlation can also be regarded as an anisotropy source. A comprehensive FORC study of $\mathbf{1}^{HT}$ and $\mathbf{1}^{HT}$D will be devoted to a future study.

DSC Measurements

$\mathbf{1}^{HT}$ and $\mathbf{1}^{HT}$D were studied by differential scanning calorimetry (DSC) over the 200–345 K temperature range (Figure 5). The thermal profile of the two complexes is very similar. They both exhibit, on warming, an endothermic peak and on cooling, an exothermic peak, whose shape is characteristics of a first-order phase transition. The peaks are separated by a wide temperature domain, which is indicative for the presence of a hysteresis loop for both compounds, as detected in SQUID measurements (Figure 1). The transition temperatures have been evaluated as $T_{max}{}^{\uparrow}$ = 321(4) K and $T_{max}{}^{\downarrow}$ = 247(4) K with ΔH = 20(1) kJ mol^{-1} and ΔS = 72.5(1) J mol^{-1} K^{-1} for $\mathbf{1}^{HT}$, and as $T_{max}{}^{\uparrow}$ = 315(1) K and $T_{max}{}^{\downarrow}$ = 249(1) K with ΔH = 16(1) kJ mol^{-1} and ΔS = 64.2(1) J mol^{-1} K^{-1} for $\mathbf{1}^{HT}$D. These transition temperatures agree rather well with those obtained by SQUID measurements, the hysteresis width being identical for $\mathbf{1}^{HT}$D (66 K), whereas for $\mathbf{1}^{HT}$ a value of 74(4) K was obtained, compared with 70 K by SQUID. The vibrational contribution to the entropy variation is evaluated as ΔS_{vib} = 59.2(1) and 31.9(1) J mol^{-1} K^{-1} for $\mathbf{1}^{HT}$ and $\mathbf{1}^{HT}$D, respectively; the electronic contribution being equal to Rln5 = 13.4 J mol^{-1} K^{-1} for Fe^{II} SCO compounds.[1b] Compounds $\mathbf{1}^{LT}$ and $\mathbf{1}^{LT}$D were also studied by DSC over the range 300–355 K. They both display a reversible first-order phase transition with transitions temperatures $T_{max}{}^{\uparrow}$ = 346 K and $T_{max}{}^{\downarrow}$ = 325 K with ΔH = 23(1) kJ mol^{-1} and ΔS = 68.7(1) J mol^{-1} K^{-1} for $\mathbf{1}^{LT}$, and $T_{max}{}^{\uparrow}$ = 345 K and $T_{max}{}^{\downarrow}$ = 322 K for $\mathbf{1}^{LT}$D with ΔH = 20(1) kJ mol^{-1} and ΔS = 61.2(1) J mol^{-1} K^{-1}.

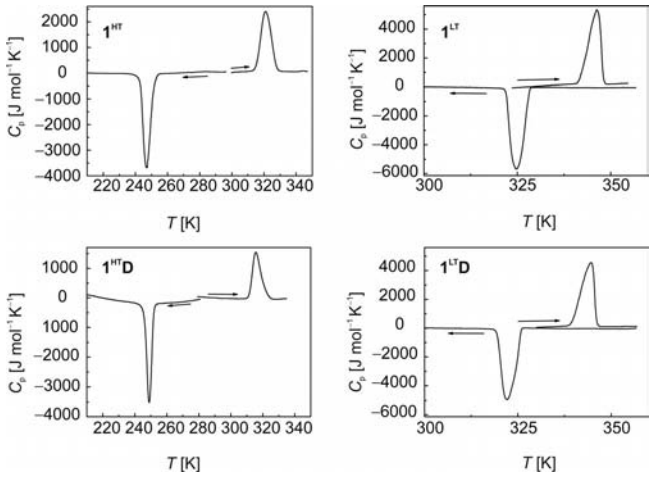

Figure 5. DSC profiles of $\mathbf{1}^{HT}$, $\mathbf{1}^{HT}$D, $\mathbf{1}^{LT}$ and $\mathbf{1}^{LT}$D in the cooling (←) and warming (→) modes.

The unusual ST behaviour of **2**·MeOH and **2**·CD_3OD was investigated by DSC at a scan rate of 10 K/min over the temperature range 120–300 K in warming and cooling modes (Figure 6). For **2**·MeOH, a steep endothermic peak was observed on warming at $T_{max}{}^{\uparrow}$ = 239 K and an exothermic peak was recorded at $T_{max}{}^{\downarrow}$ = 153 K, on cooling, thus revealing a hysteresis loop with a width of 86 K. This behaviour is characteristic of a first-order phase transition and can be related to the hysteretic ST tracked by SQUID measurements (Figure 2), with an excellent agreement regarding transition temperatures.

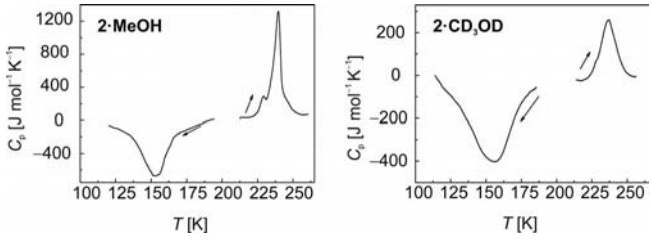

Figure 6. DSC profile of **2**·MeOH (left) and **2**·CD_3OD (right) in the 120–300 K temperature range in the cooling (←) and warming (→) modes.

The enthalpy and entropy variations associated to the phase transitions of **2** have been evaluated as ΔH = 15(1) kJ mol^{-1} and ΔS = 90.3(1) J mol^{-1} K^{-1}. For **2**·CD_3OD,

the transition temperatures were found as $T_{max}^{\uparrow}$ = 237 K and $T_{max}^{\downarrow}$ = 156 K with ΔH = 9(1) kJ mol^{-1} and ΔS = 76.3(1) J mol^{-1} K^{-1}. The entropy variation for **2**·MeOH is much larger than that of **2**·CD_3OD and, most interestingly, higher than those reported for other 1D Fe^{II} coordination polymers.[4,22] This high value calls for the presence of a structural phase transformation. Interestingly, a shoulder is detected on the endothermic peak of **2**·MeOH at $T_{max}^{\uparrow}$ = 229 K, but absent on the exothermic peak associated with the spin transition. This signal is not an artefact as it was observed in several DSC experiments in cooling and warming modes. Most interestingly, an unusual increase of $\chi_M T$ was detected in the SQUID measurements recorded on warming over the same temperature range (Figure 2a). Compound **2**·MeOH was studied by DSC on warming from 120 to 345 K (Figure 7) enabling us to fully reproduce the two endothermic signals displayed in Figure 6, which thus confirms a step in the warming branch of the ST curve of this material. The sample was then warmed and studied above room temperature allowing the detection of a steeper endothermic peak, reminiscent of both methanol release and spin-state change as confirmed by both SQUID measurements (Figure 2) and thermogravimetric analysis.

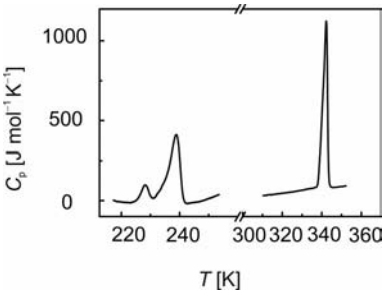

Figure 7. DSC profile of **2**·MeOH on warming over the temperature range 120–360 K.

In Table 2, the transition temperatures obtained by SQUID and DSC measurements and the thermodynamic parameters of the ST complexes are summarised. In general, a very good agreement between the transition temperatures is obtained by the two different methods. Differences (especially for $\mathbf{1}^{LT}$/$\mathbf{1}^{LT}$D) can be explained by the difference in scan rates. A comparison of the obtained entropy values reveals, that upon deuteriation, a significant decrease of the entropy is observed for all samples. In contrast, the values of the HT and LT modifications of **1** are very similar. This indicates that the hydrogen bonds (ref.[9]; see X-ray structures) significantly influence the SCO properties of the compounds presented here. The entropy values are significantly higher than the values determined for two monomeric complexes of this type of Schiff base like ligands with pyridine (37.8 kJ/mol, abrupt ST with 2 K wide hysteresis) or *N*,*N*-dimethylaminopyridine (31.5 kJ/mol, abrupt ST with 9 K wide hysteresis) as axial ligands in which no hydrogen-bond network is observed.[24] They are, however, with the exception of **2**·MeOH, in the range reported for highly cooperative 1D coordination polymers.[4,22] All these parameters indicate that, for the complexes discussed in this work, the hydrogen-bond network plays an important role for the spin transition and that most presumably the ST is associated with a structural phase transition.

Table 2. Transition temperatures recorded by SQUID and DSC measurements.

	$T_{1/2}^{\uparrow}$ [K]	$T_{1/2}^{\downarrow}$ [K]	ΔT [K]	ΔH [kJ mol^{-1}]	ΔS [J mol^{-1} K^{-1}]
$\mathbf{1}^{HT}$[a]	314	244	70		
$\mathbf{1}^{HT}$[b]	321	247	74	20(1)	72.5(1)
$\mathbf{1}^{HT}$D[a]	309	243	66		
$\mathbf{1}^{HT}$D[b]	315	249	66	16(1)	64.2(1)
$\mathbf{1}^{LT}$[a]	331	326	5		
$\mathbf{1}^{LT}$[b]	346	325	21	23(1)	68.7(1)
$\mathbf{1}^{LT}$D[a]	332	326	6		
$\mathbf{1}^{LT}$D[b]	345	322	23	20(1)	61.2(1)
2·MeOH[a]	235	153	82		
2·MeOH[b]	239	153	86	15(1)	90.3(1)
2·CD_3OD[a]	231	152	79		
2·CD_3OD[b]	237	156	81	9(1)	76.3(1)

[a] By SQUID. [b] By DSC.

X-ray Structure Analysis

Crystals suitable for X-ray structure analysis were obtained for $\mathbf{1}^{LT}$, $\mathbf{1}^{HT}$D, $\mathbf{1}^{LT}$D, **2**·MeOH and **2**·CD_3OD (the same samples as those used for the magnetic measurements in all cases). In the case of $\mathbf{1}^{LT}$D, only the cell parameters were determined. Selected bond lengths and angles as well as selected intermolecular distances are reported in Tables 3 and 4. Full refinement details are given in Table 5. For completeness, the data of $\mathbf{1}^{HT}$[9] are also given. ORTEP drawings illustrating the asymmetric units of the different modifications of **1** and **2** are given in Figures 8 and 9. The molecular structures of $\mathbf{1}^{LT}$ and $\mathbf{1}^{HT}$D were determined at 200 K and 275 K, respectively. The molecule structures of **2**·MeOH and **2**·CD_3OD could only be determined at 200 K and 173 K, respectively, as the crystals crumbled at higher/lower temperatures due to the spin transition. For each of

Table 3. Selected bond lengths [Å] and angles [°] of $\mathbf{1}^{LT}$, $\mathbf{1}^{HT}$,[9] $\mathbf{1}^{HT}$D, **2**·MeOH and **2**·CD_3OD within the first coordination sphere.

Compound	Fe–N1/2 [Å]	Fe–O1/2 [Å]	Fe–N3/5 [Å]	O1–Fe–O2 [°]	N3–Fe–N5 [°]
$\mathbf{1}^{LT}$	1.879(2)/1.890(2)	1.951(2)/1.929(2)	1.989(2)/2.011(3)	88.26(8)	178.9(1)
$\mathbf{1}^{HT}$[9]	2.086(3)/2.079(4)	2.048(3)/2.010(3)	2.196(4)/2.241(3)	108.0(1)	173.8(1)
$\mathbf{1}^{HT}$D	2.096(2)/2.092(2)	2.052(2)/2.013(2)	2.195(3)/2.242(2)	108.22(8)	173.5(1)
Compound	Fe–N1/2	Fe–O1/2	Fe–N3/4	O1–Fe–O2	N3–Fe–N4
2·MeOH	2.093(3)/2.092(3)	2.011(2)/2.020(2)	2.271(3)/2.245(3)	109.70(8)	177.05(9)
2·CD_3OD	2.091(4)/2.096(5)	2.014(4)/2.017(4)	2.260(5)/2.231(5)	109.41(16)	176.99(19)

these materials, structural analysis revealed a distorted octahedral iron(II) environment consisting of equatorially coordinating tetradentate Schiff base like ligand and two axially coordinating ligands with a *N*-heterocycle. In the case of **1**, the two monodentate axial imidazole ligands led to mononuclear complexes. In the case of **2**, each bidentate 4,4′-azopyridine ligand bridges two iron(II) centres and thus propagates to form extended 1D chains. The complexes $\mathbf{1}^{HT}$[9] and $\mathbf{1}^{HT}$D crystallise with monoclinic symmetry. Both complexes are isostructural with the average bond lengths and angles of the inner coordination sphere around the iron centre in the region typically reported for

Table 4. Selected intermolecular distances [Å] of the three modifications $\mathbf{1}^{HT}$ (275 K), $\mathbf{1}^{HT}$D (275 K) and $\mathbf{1}^{LT}$ (200 K) and of the two modifications **2**·MeOH and **2**·CD_3OD. For $\mathbf{1}^{HT}$ and $\mathbf{1}^{HT}$D an infinite 2D hydrogen-bond network with the base vectors: [0 1 0] and [0 0 1] along the plane: (1 0 0) with additional weak contacts between the single planes is obtained. For the compound $\mathbf{1}^{LT}$, an infinite 3D hydrogen-bond network with the base vectors: [1 0 0], [0 1 0], [0 0 1] is observed.

Compound		D–H	H···A	D···A	D–H···A
$\mathbf{1}^{HT}$[3]	N(4)–H(4)···O(1)[a]	0.86	2.00	2.832(5)	161
	N(6)–H(66)···O(5)[b]	0.86	1.98	2.841(4)	176
$\mathbf{1}^{HT}$D	N(5)–D(5)···O(1)[a]	0.86	2.02	2.847(4)	162
	N(6)–D(6)···O(5)[b]	0.86	1.99	2.846(3)	177
$\mathbf{1}^{LT}$	N(6)–H(6A)···O(6)[c]	0.88	2.01	2.832(3)	155
	N(5)–H(5A)···O(1)[d]	0.88	2.10	2.950(3)	162
	N(5)–H(5A)···O(2)[d]	0.88	2.39	2.945(3)	121
	C(22)–H(22)···O(4)[e]	0.95	2.57	3.520(4)	178
	C(16)–H(16B)···O(6)[f]	0.99	2.56	3.508(4)	161
2·MeOH	O(5)–H(5A)···O(3)	0.84	2.03	2.865(4)	174
	C(32)–H(32)···O(4)[b]	0.95	2.57	3.415(5)	148
	C(35)–H(35)···O(3)[g]	0.95	2.42	3.331(49)	161
	C(39)–H(39B)···O(1)[h]	0.98	2.53	3.346(5)	141
2·CD_3OD	O(5)–D(5)···O(3)	0.84	2.03	2.867(8)	171
	C(32)–H(32)···O(4)[j]	0.95	2.57	3.416(9)	148
	C(35)–H(35)···O(3)[i]	0.95	2.42	3.329(8)	161
	C(39)–D(39A)···O(1)[k]	0.98	2.50	3.344(8)	144

[a] $-x$, $1/2 + y$, $-1/2 - z$. [b] $-x$, $-1 - y$, $-z$. [c] $2 - x$, $1/2 + y$, $5/2 - z$. [d] $1/2 + x$, $5/2 - y$, $2 - z$. [e] $2 - x$, $-1/2 + y$, $5/2 - z$. [f] $1 + x$, $1 + y$, z. [g] $-1 + x$, y, z. [h] $1 - x$, $-y$, $-z$. [i] $1 + x$, y, z. [j] $1 - x$, $2 - y$, $2 - z$. [k] $-x$, $1 - y$, $2 - z$.

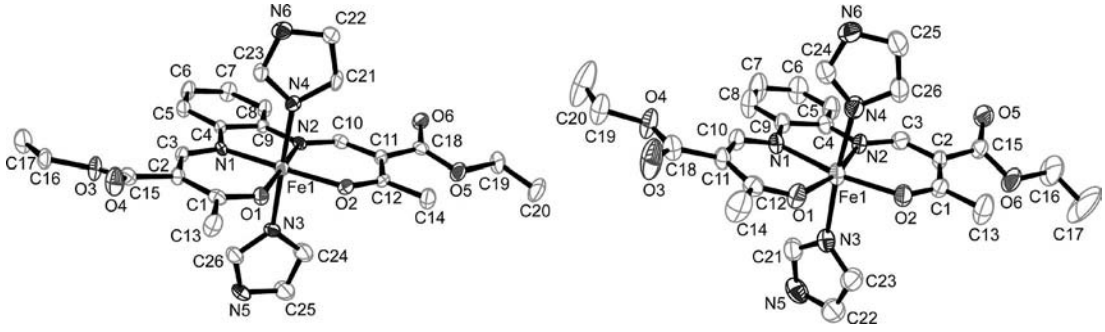

Figure 8. ORTEP drawing of the asymmetric units of compounds $\mathbf{1}^{LT}$ at 200 K (left) and $\mathbf{1}^{HT}$D at 275 K (right).

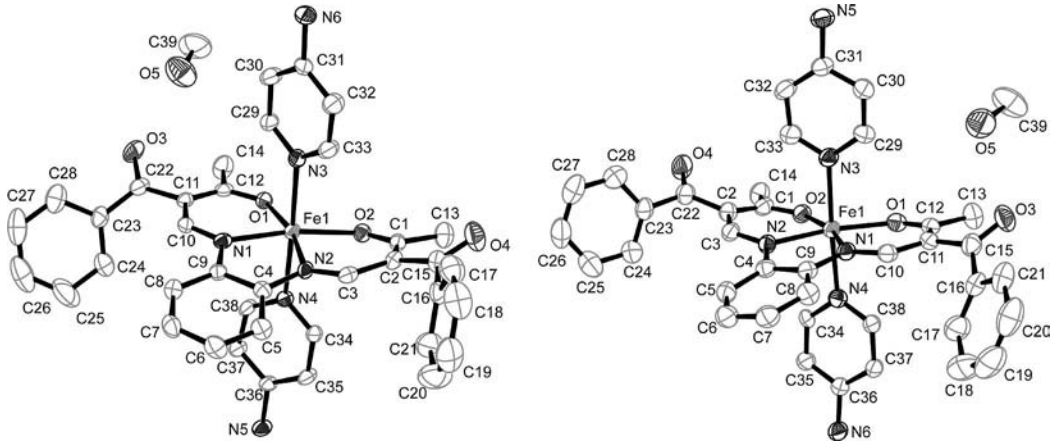

Figure 9. ORTEP drawing of the asymmetric units of compounds **2**·MeOH (left) and **2**·CD_3OD (right).

HS iron(II) complexes of this ligand type [2.09 Å ($Fe–N_{eq}$), 2.03 Å ($Fe–O_{eq}$), 2.22 Å ($Fe–N_{ax}$) and 108° (O–Fe–O)].[25,26] The complexes $\mathbf{1}^{LT}$ and $\mathbf{1}^{LT}$D crystallise with orthorhombic symmetry. For $\mathbf{1}^{LT}$, the average bond lengths and angles of the inner coordination sphere around the iron centre [1.88 Å ($Fe–N_{eq}$), 1.94 Å ($Fe–O_{eq}$), 2.00 Å ($Fe–N_{ax}$) and 88° (O–Fe–O)] are in the region reported previously for similar LS iron(II) complexes – in full agreement with the results of the susceptibility measurements.[25,26] No values give an indication why such pronounced differences are observed between the ST values of the two modifications. A detailed analysis of the intermolecular interactions can provide an answer to this question. The complexes **2**·MeOH and **2**·CD_3OD crystallise with triclinic symmetry and have one iron(II) centre in the asymmetric unit. The parallel 1D chains of both complexes propagate along the [1 –1 –2] direction and are stacked such that there is a solvent accessible void volume for one methanol molecule per iron(II) centre. Both complexes are isostructural. The average bond lengths around the iron centre [**2**·MeOH: 2.09 Å ($Fe–N_{eq}$), 2.02 Å ($Fe–O_{eq}$), 2.26 Å ($Fe–N_{ax}$); **2**·CD_3OD: 2.09 Å ($Fe–N_{eq}$), 2.01 Å ($Fe–O_{eq}$), 2.25 Å ($Fe–N_{ax}$)] and the O–Fe–O angle (**2**·MeOH: 110°; **2**·CD_3OD: 109°) are indicative of iron(II) in the HS state.[25,26]

Intermolecular Investigations

In contrast to $\mathbf{1}^{HT}$,[9] the packing of the molecules of $\mathbf{1}^{LT}$ in the crystal (Figure 10) reveals three different hydrogen bonds between neighbouring molecules. The one involving the NH hydrogen atom (H6A) of the imidazole unit and the *O*COEt oxygen atom (O6) of the equatorial ligand is comparable to that observed in the $\mathbf{1}^{HT}$ structure.[9] The second one involving the NH hydrogen atom (H5A) and the coordinated carbonyl oxygen atom (O1) of the equatorial ligand is significantly weaker than the second hydrogen bond in $\mathbf{1}^{HT}$ (A···D 2.95 Å instead of 2.83 Å in the $\mathbf{1}^{HT}$ modification).[9] This is probably due to the third hydrogen bond that also involves the NH hydrogen atom (H5A) and the coordinated carbonyl oxygen atom (O2) of the equatorial ligand. One could argue that those two hydrogen bonds are the reason for the higher transition temperature of $\mathbf{1}^{LT}$. Upon spin transition the equatorial ligand expands; this is reflected by an increase in the value of the O1–Fe–O2 angle. This angle, however, is to some extent fixed by the bridging hydrogen bond and by this the LS state of the complex is stabilised compared with $\mathbf{1}^{HT}$. The combination of the three hydrogen bonds leads to an infinite 3D network of linked molecules. Some additional weak contacts between the imidazole CH (H22) and the *O*COEt oxygen atom (O4) and the hydrogen atom of the ethoxy group of the equatorial ligand (H16B) and the OC*O*Et oxygen atom (O6) are also involved in the hydrogen-bonding network. For $\mathbf{1}^{HT}$, three additional weak contacts were obtained; two of them involving the same donor atom, the total number of short contacts is the same for both modifications of **1**. The details for all intermolecular contacts are given in Table 4. The first suggestion would be that the 3D hydrogen-bond network of $\mathbf{1}^{LT}$ should lead to wider hysteresis loops, quite contrary to the experimental results. This discrepancy can be explained by the significantly weaker hydrogen bonds between the N5 hydrogen and O1/O2. Additionally, the stabilisation of the LS state due to this bridging hydrogen bond can account for the small hysteresis loop in $\mathbf{1}^{LT}$.

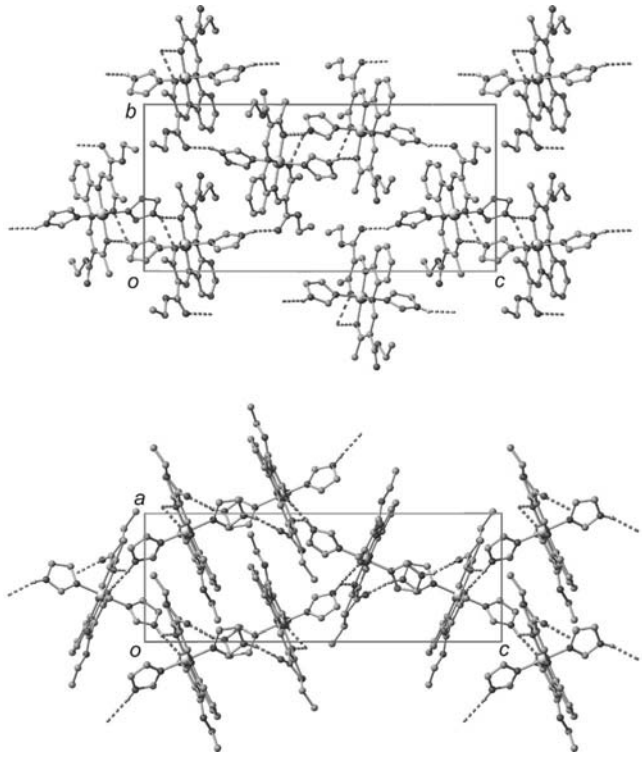

Figure 10. Packing of compound $\mathbf{1}^{LT}$ in the crystal at 200 K. Top: view along [100], bottom: view along [010].

The molecular packing of **2**·MeOH and **2**·CD_3OD (Figure 11) reveals four hydrogen bonds between adjacent chains, which are identical when comparing the two modifications. Most obvious is the hydrogen bond formed between the hydroxy group of the methanol molecule and the carbonyl oxygen atom O3 of the equatorial ligand. Moreover, three non-classical hydrogen bonds of the type C–

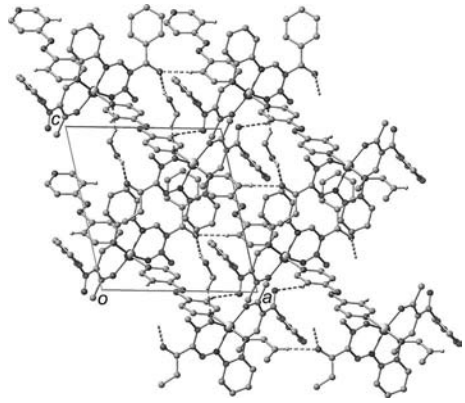

Figure 11. Packing of compounds **2**·MeOH in the crystal. View along [010].

H···O are found. Two of which involve the carbonyl oxygen atoms O3 and O4 as H-acceptor and two CH-groups of the pyridyl-rings of the axial ligand (C–H32, C–H35) act as H-donors. The third non-classical hydrogen bond involves carbonyl oxygen atom O1, which is also directly coordinated to the iron(II) centre and a proton of the methyl group of the included methanol molecule. This weak hydrogen bond is similar to the hydrogen bonds observed in the different modifications of **1** that also include the oxygen atom O1 that is coordinated to the iron centre. As for **1**, a H/D exchange leads to differences in the hysteresis width suggesting a similar mechanism in both cases.

Discussion

Labeling Experiments

For the different systems investigated in this work (**1**^{HT}/**1**^{HT}D, **1**^{LT}/**1**^{LT}D and **2**·MeOH/**2**·CD_3OD) the H/D exchange influences the width of the thermal hysteresis loop, whereas the shape of the transition curve remains unchanged. In the case of **1**^{HT}/**1**^{HT}D and **2**·MeOH/**2**·CD_3OD, the width of the hysteresis loop is reduced upon deuteriation and the transition temperatures are shifted to lower temperatures, whereas for **1**^{LT}/**1**^{LT}D the transition temperature is shifted to higher temperatures and the hysteresis width is increased. A H/D isotope effect on $T_{1/2}$ was already observed for the coordination polymer [Fe(pyridine)$_2$][Ni(CN)$_4$] by Kitazawa, Bousseksou and co-workers[27] (shift to lower temperatures) or for the mononuclear system [Fe(2-pic)$_3$]Cl$_2$·Sol (2-pic = 2-picolylamine, Sol = C_2H_5OD and CH_3OD) (shift to higher temperatures) by Gütlich et al.[28] As different electronic and vibrational factors contribute to the relative energies of the HS and the LS state, the direction of the H/D effect on $T_{1/2}$ is difficult to predict. A possible explanation for the observed effects concerning the hysteresis loop width can be related to the higher N–D bond strength compared with the N–H bond[29] and consequently the hydrogen bond strength decreases upon H/D exchange[30] leading to weaker intermolecular interactions. This is in agreement with a comparison of the cell parameters of **1**^{HT} and **1**^{HT}D, which reveals that for the deuteriated sample, all cell parameters are slightly larger; the most pronounced difference is found for the *c*-axis with a value of 27.37 instead of 27.25 Å. As the 2D hydrogen-bond network runs along the *b*/*c*-axis this agrees well with the weaker hydrogen bonds in **1**^{HT}D. The intermolecular hydrogen bonds in the deuteriated sample are slightly longer than in the previously reported complex. Nevertheless, the effect is negligible for the one involving the NH/D atom (H66/D6) of the imidazole unit and the *O*COEt oxygen atom (O5) of the equatorial ligand. In contrast, the difference between the second hydrogen bond between the NH/D atom (H4/D5) of the imidazole unit and the coordinated carbonyl oxygen atom (O1) of the equatorial ligand is more pronounced (A···D 2.85 compared with 2.83 Å in the **1**^{HT} modification). For the second pair **2**·MeOH/**2**·CD_3OD, however, no such pronounced differences were observed, but the effect on the transition curve is similar, whereas for **1**^{LT}/**1**^{LT}D a different trend is observed. A comparison of **1**^{HT} and **2**·MeOH complicates the situation even more. Here strong differences in the hydrogen-bond network are observed, but the width of the hysteresis loop is in the same order of magnitude. For **1**^{HT}, direct hydrogen bonds between the complex molecules are observed whereas for **2**·MeOH it is highly likely that the interactions mediated over the solvent molecule methanol are responsible for the wide hysteresis loop. The MeOH/CD_3OD exchange influences the width of the hysteresis loop and the loss of the methanol results in a gradual spin transition. In contrast, a comparison of **1**^{HT} and **1**^{LT} reveals a very similar hydrogen-bond network, but strong differences in the width of the hysteresis loop.

The different degrees of cooperative interactions cannot be directly correlated with the number and strength of hydrogen bonds. Several examples suggested that this is possible for the number of short van der Waals contacts.[6] For this purpose, we suggested the introduction of an quantitative parameter, the crystal contact index (CCI) that is the sum of all short and weighted contacts.[31] We assumed that every short contact (shorter than the sum of the van der Waals radii) contributes to the interactions mediating the cooperative effect. Those that are very short contribute more to the cooperative effect than those that are longer. Although this concept works rather nicely for several complexes of the family discussed in this work and also for other ST complexes,[31] it fails as soon as hydrogen bonds are involved in the intermolecular interactions. The values obtained for **1**^{HT} (4.1), **1**^{HT}D (4.0) and **1**^{LT} (4.2) are of the same order of magnitude, thus the hysteresis width does not correlate with the number of short contacts.[31] Moreover, the value for **2**·MeOH (1.7) is significantly lower, despite the even larger hysteresis loop. Nevertheless, the importance of the hydrogen bonds in connection with the wide hysteresis loops cannot be put into question as it is underlined by the DSC results in which a significant decrease of the entropy is observed upon deuteriation for all complexes. The FORCs analysis of 1^{HT} also indicates strong interactions within the 2D layer of hydrogen-bond-linked molecules as origin of the wide hysteresis loops.

To obtain a better understanding of the influence of the hydrogen bonds on the hysteresis width, their influence on the ligand field strength was considered.

Influence of Hydrogen Bonding on the Ligand Field Strength

The general idea that hydrogen bonds to atoms in close vicinity to the metal centre are responsible for variations in the crystal field was already suggested in 1978 for the iron(III) complex [Fe(saen)$_2$]Cl·H_2O.[10] The four amine hydrogen atoms of the saen ligand [saen = *N*-(2-aminoethyl)-salicylaldiminato, Scheme 3] are involved in four interactions, three with chloride ions and one with the water molecule. The complex is LS but becomes HS when dehydrated

or in solution.[10] This observation was explained with a slight increase in electron density on the amine nitrogen due to the hydrogen bond, resulting in an enhanced crystal field experienced by the central metal ion.[10] A similar observation was made for a series of iron complexes of H_2L3 [H_2L3 = 2,6-bis(pyrazol-3-yl)pyridine, Scheme 3] with varying counterions and water molecules of the general formula $[Fe(H_2L3)_2](X)_2 \cdot nH_2O$ with X = BF_4^-,[32] I^-,[32c] SCN^-,[12] $SeCN^-$[12b] and $CF_3SO_3^-$.[13] An increasing amount of water of crystallisation resulted in the stabilisation of the LS state, for example, the crystals of the BF_4^- salt with three water molecules of crystallisation are LS (no magnetic measurements), the powder sample with two water molecules of crystallisation shows a gradual ST with $T_{1/2} \approx 300$ K, whereas the water-free powder sample shows an abrupt ST with $T_{1/2}\downarrow = 170$ K and $T_{1/2}\uparrow = 180$ K.[32] In the X-ray structure analyses, hydrogen bonds were observed between the uncoordinated NH of the pyrazole ring and water, as well as the counterions. The authors assume that the hydrogen-bonded water molecules stabilise the LS state by increasing the electron density at the imine nitrogen.[32] For two of the complexes $[Fe(H_2L3)_2](SCN)_2 \cdot 2H_2O$[12] and $[Fe(H_2L3)_2](CF_3SO_3)_2 \cdot H_2O$,[13] step-wise spin transitions with hysteresis loop were obtained. In both cases, the step does not occur at $\gamma_{HS} = 0.5$, as for the example **2**·MeOH/CD_3OD in this paper. In the case of the thiocyanate salt, after the first cycling, a second phase with a one-step ST was obtained. A disruption of the hydrogen-bond network associated with a reversible crystallographic change is assumed to be the origin of the unusual ST behaviour.[12] A structural phase transition and the associated modification of the hydrogen-bond network are discussed as being responsible for the step ST with hysteresis of the compound FeH_4L4.[15] Significant differences in the transition temperature of $[FeH_2L5(py)_2] \cdot py$ in the solid state ($T_{1/2} >$ 350 K) and in solution ($T_{1/2} \approx 200$ K, both gradual spin transitions) were also associated with the hydrogen-bond network observed in the X-ray structure.[11] Such observations are not limited to monomeric complexes. For the 1D chain material $[Fe(NH_2trz)_3](NO_3)_2$, the 33 K wide thermal hysteresis loop is associated with a network of hydrogen bonds,[22,33] and for the very similar $[Fe(Htrz)_2(trz)](BF_4)$, an extended network of hydrogen bonds had been singled out to be the origin of the 40 K large hysteresis above room temperature.[4,34] A detail X-ray structure analysis on the 2D network of $[Fe(btr)_2(NCS)_2] \cdot H_2O$ reveals that the HS→LS transition reduces the O–H···N contacts between the water molecules and the free N atoms of the triazole ligand. Those changes and the rigid nature of the bridging ligand are made responsible for the observed highly cooperative SCO behaviour (25 K wide hysteresis).[20,21] All these examples demonstrate that (i) hydrogen bonds significantly influence the ligand field strength if donor atoms or atoms in conjugated systems with donor atoms are involved and (ii) changes in the hydrogen-bond network (often, but not necessarily, in line with a structural phase transition) result in changes in the ST behaviour. This information can now be used to suggest a new model for the explanation of the wide thermal hysteresis loops of the high-temperature modification of **1** and **2**·MeOH (as well as the different literature examples with hysteresis loops in which hydrogen bonding is observed).

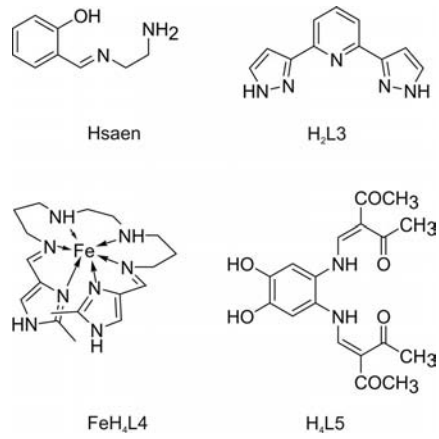

Scheme 3. Schematic representation of ligands and complexes with potential for hydrogen bonding: Hsaen from ref.[10], H_2L3 from ref.[12,13,33], FeH_4L4 from ref.[13] and H_4L5 from ref.[11]

A ST is associated with changes in the bond length between the iron centre and the donor atoms. These changes most likely influence the strength of the hydrogen bond to the donor atom, for example, in the case of $\mathbf{1}^{HT}$ between the NH of the imidazole ligand and O1 of the equatorial ligand. This change influences the overall ligand field strength of the complex. In our two cases, upon cooling, this change results in a stabilisation of the LS state (corresponding to a shift of the LS potential wells to lower energies; Scheme 4). As a consequence, ΔE_{HL} increases and a higher transition temperature is observed in the heating mode. Wide thermal hysteresis loops should thus be observed if a large enough change in a hydrogen-bond network involving donor atoms or atoms in conjugated systems with donor atoms is observed. Those changes can be

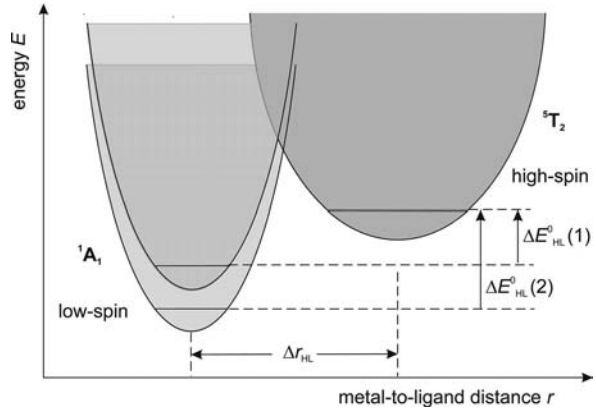

Scheme 4. Schematic representation of the HS and LS potential wells before spin transition (LS dark grey) and after spin transition (LS light grey). Upon spin transition, a change in the hydrogen-bond strength results in a different ligand field strength for the LS state and therefore a higher ΔE_{HL} that leads to a higher transition temperature in the heating mode compared with the cooling mode.

associated with reversible structural phase transitions. The second question to be addressed in this context is that of domain formation as the reason for hysteresis loops (the theory of Sorai and Seki).[35] The high interaction parameter J of 560 K derived from FORC analysis indicates a pronounced intradomain interaction. A possible explanation to unify both concepts would be that one domain is formed by an assembly of molecules with the same ligand field strength or, if a structural phase transition takes place, of the same structural phase. This implies that both theories not only coexist but also support each other. Further investigations on the compounds presented in this work and on new examples are necessary to verify this concept.

Conclusion

Spin-transition molecular materials have a high potential as materials for various applications in display and data processing (memory device units, cold channel control units in food and medical storage devices). These potential applications desire a highly cooperative ST system with an approximate 100 K wide hysteresis loop.[2a] In this manuscript, we have introduced a new concept to explain the interplay of wide bistability domains and hydrogen bonds between the magnetic centres. This concept brings us one step closer to the application of SCO materials.

Experimental Section

General Synthesis: All syntheses were carried out under argon using Schlenk tube techniques. Methanol was purified and distilled under argon before use. [FeL1(MeOH)$_2$] and [FeL2(MeOH)$_2$] were prepared as described in literature[36] using anhydrous iron(II) acetate as starting material.[37] Imidazole was purchased from Alfa Aesar, [D$_4$]imidazole (98 atom-%) [D$_1$]methanol (CH$_3$OD, 99.5 atom-%) and [D$_4$]methanol (HDO + D$_2$O < 0.03%) were purchased from Aldrich and used as received.

[FeL1(HIm)$_2$] (1^{LT}): A mixture of [FeL1(MeOH)$_2$] (0.09 g, 0.18 mmol) and imidazole (0.30 g, 4.41 mmol) was dissolved in methanol (8.0 mL) and refluxed for 5 min. After cooling, the solution was allowed to stand for three days until a fine crystalline black precipitate was obtained, which was filtered off, washed with methanol (2 × 5 mL) and dried in vacuo (yield: 0.05 g, 48%). IR (KBr): $\tilde{\nu}$ = 1702 (s), 1575 cm^{-1} (s). $C_{26}H_{30}FeN_6O_6$ (578.41): calcd. C 53.99, H 5.23, N 14.53; found C 53.79, H 5.23, N 14.55.

[FeL1(HIm)$_2$] (1^{HT}): A mixture of [FeL1(MeOH)$_2$] (0.56 g, 1.11 mmol) and imidazole (3.80 g, 55.5 mmol) was dissolved in methanol (20 mL) and refluxed for 5 min. After cooling, the fine crystalline black precipitate was filtered off immediately, washed with methanol (2 × 5 mL) and dried in vacuo (yield: 0.43 g, 67%). IR (KBr): $\tilde{\nu}$ = 1703, 1672, 1620 cm^{-1} (s). MS [DEI-(+), 70 eV]: *m*/*z* (%) = 442 (64) [FeL1$^+$], 68 (100) [HIm$^+$]. $C_{26}H_{30}FeN_6O_6$ (578.41): calcd. C 53.99, H 5.23, N 14.53; found C 53.97, H 5.03, N 14.45.

[FeL1([D$_4$]imidazole)$_2$] (1^{HT}D): The synthesis was carried out in a similar manner as described above. A mixture of [FeL1(MeOH)$_2$] (0.13 g, 0.26 mmol) and [D$_4$]imidazole (0.93 g, 12.8 mmol) was dissolved in [D$_1$]methanol (6.1 mL) and refluxed for 5 min. After cooling, the fine crystalline black precipitate was immediately filtered off to give **1**^{HT}D (yield: 0.06 g, 38%). IR (KBr): $\tilde{\nu}$ = 1688 (s), 1671 (m), 1563 cm^{-1} (vs). MS [DEI(+), 70 eV]: *m*/*z* (%) = 442 (80) [FeL1$^+$], 72 (100) [$C_3D_4N_2^+$]. $C_{26}H_{22}D_8FeN_6O_6$ (586.46): calcd. C 53.25, N 14.33; found C 53.14, N 14.16.

[FeL1([D$_4$]imidazole)$_2$] (1^{LT}D): The mother liquor from the synthesis of **1**^{HT}D was kept refrigerated at 4 °C. After two days **1**^{LT}D precipitated as fine black needles, which were filtered off and dried in vacuo (yield: 0.02 g, 13%). Unit cell (T = 200 K): orthorhombic *P*, a = 8.88, b = 11.76, c = 24.78, V = 2587.6. IR (KBr): $\tilde{\nu}$ = 1688 (w), 1671 (s), 1562 cm^{-1} (vs). MS [DEI-(+), 70 eV]: *m*/*z* (%) = 442 (49) [FeL1$^+$], 72 (100) [$C_3D_4N_2^+$]. $C_{26}H_{22}D_8FeN_6O_6$ (586.46): calcd. C 53.25, N 14.33; found C 52.97, N 15.34.

4,4′-Azopyridine (azpy): 4,4′-Azopyridine was prepared by the oxidative coupling of 4-aminopyridine and hypochlorite, using an adaptation of the method of Launay et al.[38] A cold solution of 4-aminopyridine (5.05 g, 53.7 mmol) in water (100 mL) was added dropwise to a 6.5% NaOCl solution (300 mL). The mixture was stirred at 5 °C, during which time an orange precipitate formed. After completion of the addition, the reaction mixture was stirred for another 15 min. The precipitate was filtered off and washed with cold water. The aqueous phase was extracted three times with diethyl ether. The combined organic phases were dried using $MgSO_4$ and the solvent evaporated. The crude products were recrystallised from water yielding 4,4′-azopyridine as orange needles (yield: 1.70 g, 34%). ^{1}H NMR (270 MHz, $CDCl_3$, 25 °C, TMS) δ = 8.92 (m, 4 H, Ar-H), 7.69 (m, 4 H, Ar-H) ppm. MS [DEI-(+), 70 eV]: *m*/*z* (%) = 184 (55) [M$^+$], 78 (100) [$C_5H_4N^+$]. $C_{10}H_8N_4$ (184.20): calcd. C 65.21, H 4.38, N 30.42; found C 64.67, H 4.20, N 30.18.

[FeL2(azpy)]·MeOH (2·MeOH): **2**·MeOH was synthesised by a slow diffusion technique using a Schlenk tube that is, to a certain height, separated into two chambers. Into one chamber [FeL2(MeOH)$_2$] (0.09 g, 0.16 mmol) was placed and into the other chamber 4,4′-azopyridine (0.03 g, 0.17 mmol) was placed. Methanol was carefully added to the point to allow slow diffusion at one point of contact. Within a couple of days, **2**·MeOH was obtained as black crystals, which were of sufficient quality for X-ray analysis. After removing the solvent the product was dried in vacuo and kept refrigerated at 4 °C (yield: approximately 0.10 g, 85%). IR (KBr): $\tilde{\nu}$ = 1627 (s), 1554 cm^{-1} (vs). MS [DEI-(+), 70 eV]: *m*/*z* (%) = 506 (24) [FeL2$^+$], 184 (73) [azpy$^+$], 78 (100) [$C_5H_4N^+$]; DTG: up to 150 °C: –2.12% = loss of 1 methanol (calcd.: 4.4%; presumably part of the methanol was lost during the storage of the sample). $C_{39}H_{34}FeN_6O_5$ (722.58): calcd. C 64.83, H 4.74, N 11.63; found C 65.03, H 4.70, N 11.81.

[FeL2(azpy)]·CD$_3$OD (2·CD$_3$OD): **2**·CD$_3$OD was synthesised by slow diffusion just as **2**·MeOH. [FeL2(MeOH)$_2$] (0.09 g, 0.16 mmol) and 4,4′-azopyridine (0.03 g, 0.17 mmol) were dissolved in [D$_4$]methanol. Within a couple of days, **2**·CD$_3$OD was obtained in form of black crystals, which were of sufficient quality for X-ray analysis. After removing the solvent the product was dried in vacuo and kept refrigerated at 4 °C (yield: approximately 0.10 g, 85%). IR (KBr): $\tilde{\nu}$ = 1627 (s), 1555 cm^{-1} (vs). MS [DEI-(+), 70 eV]: *m*/*z* (%) = 506 (10) [FeL2$^+$], 184 (59) [azpy$^+$], 78 (100) [$C_5H_4N^+$]; DTG: up to 150 °C: –3.7% = loss of 1 [D$_4$]methanol (calcd.: 4.9%). $C_{39}H_{30}D_4FeN_6O_5$ (726.61): calcd. C 64.47, N 11.57; found C 64.52, N 11.73.

[FeL2(azpy)](2): [FeL2(MeOH)$_2$] (0.12 g, 0.21 mmol) and 4,4′-azopyridine (0.31 g, 1.66 mmol) were dissolved in methanol (15 mL) and refluxed for 1 h. The product precipitated from the boiling solution as black powder. After cooling to room temperature **2** was filtered off, washed with methanol (5 mL) and dried in vacuo

Table 5. Crystallographic data of compound $\mathbf{1}^{LT}$, $\mathbf{1}^{HT}$D, **2**·MeOH and **2**·CD_3OD. For comparison purposes, the data for $\mathbf{1}^{HT}$[9] are also given.

Compound	$\mathbf{1}^{HT}$[9][a]	$\mathbf{1}^{HT}$D	$\mathbf{1}^{LT}$	**2**·MeOH	**2**·CD_3OD
Formula	$C_{26}H_{30}FeN_6O_6$	$C_{26}H_{24}D_6FeN_6O_6$	$C_{26}H_{30}FeN_6O_6$	$C_{39}H_{34}FeN_6O_5$	$C_{39}H_{30}D_4FeN_6O_5$
M_r [g mol^{-1}]	578.41	584.45	578.41	722.57	726.60
Crystal system	monoclinic	monoclinic	orthorhombic	triclinic	triclinic
Space group	$P2_1/c$	$P2_1/c$	$P2_12_12_1$	$\bar{P}$ 1	$\bar{P}$ 1
λ [Å]	0.71073	0.70930	0.70930	0.71069	0.71073
T [K]	275(2)	275(2)	200(2)	200(2)	173(2)
Crystal size [mm]	0.14 × 0.03 × 0.03	0.13 × 0.13 × 0.06	0.47 × 0.14 × 0.08		0.38 × 0.20 × 0.14
a [Å]	11.6280(12)	11.653(3)	8.8957(8)	11.747(7)	11.7410(6)
b [Å]	9.3700(8)	9.375(3)	11.743(2)	12.103(6)	12.1271(7)
c [Å]	27.245(2)	27.306(5)	24.832(9)	13.852(9)	13.8360(8)
α [°]	90	90	90	114.173(6)	114.181(3)
β [°]	112.037(4)	112.136(15)	90	101.169(5)	101.169(3)
γ [°]	90	90	90	92.309(4)	92.240(4)
V [Å^3]	2751.6(4)	2763.2(12)	2594.0(11)	1746.9(18)	1747.63(17)
Z	4	4	4	2	2
$d_{calcd.}$ [g cm^{-1}]	1.396	1.405	1.481	1.374	1.381
μ [mm^{-1}]	0.599	0.596	0.635	0.485	0.485
Absorption correction	none	none	none	multiscan	multiscan
Reflections collected	5295	30838	11093	20384	10482
Indep. reflections (R_{int})	3878 (0.0445)	4102 (0.0920)	4542 (0.0538)	11225 (0.1186)	6269 (0.0379)
Data/restrains/parameters	3878/0/356	4102/0/356	3174/0/356	11225/0/455	6269/0/463
$R1$[b] [$I>2\sigma(I)$] (all data)	$R1$ = 0.0555 (0.0946)	$R1$ = 0.0400 (0.0921)	$R1$ = 0.0367 (0.0600)	$R1$ = 0.0652 (0.1287)	$R1$ = 0.0785 (0.1014)
$wR2$[c] [$I>2\sigma(I)$] (all data)	$wR2$ = 0.1268 (0.1470)	$wR2$ = 0.0579 (0.0646)	$wR2$ = 0.0586 (0.0632)	$wR2$ = 0.1338 (0.1540)	$wR2$ = 0.2085 (0.2201)
GooF	1.012	0.848	0.925	0.924	1.173

[a] For a better comparison of the different structures the data of the previously published complex $\mathbf{1}^{HT}$ (ref.[9]) were translated from $P2_1/n$ to $P2_1/c$. [b] $R1 = \Sigma||F_o| - |F_c||/\Sigma|F_o|$. [c] $wR2 = \{\Sigma[w(F_o^2 - F_c^2)^2]/\Sigma w(F_o^2)^2\}^{1/2}$, $w = 1/[\sigma^2(F_o^2) + (aP)^2 + bP]$, where $P = [F_o^2 + 2(F_c^2)]/3$.

(0.09 g, 61%). IR (KBr): $\tilde{\nu}$ = 1627 (m), 1556 cm^{-1} (vs). MS [DEI-(+), 70 eV]: m/z (%) = 506 (9) [FeL2$^+$], 184 (43) [azpy$^+$], 78 (100) [$C_5H_4N^+$]. $C_{38}H_{30}FeN_6O_4$ (690.54): calcd. C 66.10, H 4.38, N 12.17; found C 65.34, H 4.73, N 12.12.

Magnetic Measurements: Were performed on a Quantum-Design-MPMSR-XL-SQUID-Magnetometer in the 50 – 400 K temperature range at 0.05 T in the settle mode. The data corrections were made using tabulated Pascal's constants. All measurements were reproduced twice. The FORC distribution is determined at each point by fitting a mixed second-order polynomial of the form [$a_1 + a_2T_a + a_3T_b + a_4T_a^2 + a_5T_b^2 + a_6T_aT_b$] to a local moving grid. When interpolation is done to obtain the distribution value, we also take into consideration the neighbouring interpolated point. In this case, the value of $-a_6$ provides the mixed second derivative of the fitted surface and it can be assigned to the centre of grid as a representation of the density of the FORC distribution $\rho(T_a,T_b)$ at that point. The value of the magnetisation is interpolated in every measured point with that polynomial of second order.

Differential Scanning Calorimetric Measurements: Were carried out in a $He_{(g)}$ atmosphere using a Perkin–Elmer DSC Pyris 1 instrument equipped with a cryostat and operating down to 98 K. An aluminium capsule was loaded with 10–30 mg of sample and hermetically sealed. The heating and cooling rates were fixed at 10 K min^{-1}. Temperatures and enthalpies were calibrated over the temperature range of 298–400 K using the solid–liquid transitions of pure Indium (99.99%)[39] and the crystal–crystal transitions of pure cyclopentane (≥ 99%)[40] over the range 120–298 K. The sample was maintained at room temperature or at the highest temperature for 5 min to allow the system to equilibrate and was then further warmed or cooled in the region of interest. The experiments were carried out four times to confirm reproducibility.

Crystal Structure Analysis: The intensity data of $\mathbf{1}^{LT}$, $\mathbf{1}^{HT}$D and **2**·MeOH were collected on an Oxford XCalibur diffractometer, the intensity data of **2**·CD_3OD were collected on a Nonius Kappa CCD diffractometer, both using graphite-monochromated Mo-K_α radiation. The data were corrected for Lorentz and polarisation effects. The structure was solved by direct methods (Sir 97[41]) and refined by full-matrix least-square techniques against F_0^2 (SHELXL-97[42]). The hydrogen atoms were included at calculated positions with fixed thermal parameters. Cell parameters and refinement results are summarised in Table 5.[43] ORTEP-III was used for structure representation.[44] Crystallographic data for the structures reported in this paper have been deposited with the Cambridge Crystallographic Data Centre as supplementary publication no. CCDC-723037 ($\mathbf{1}^{HT}$D), -723038 ($\mathbf{1}^{LT}$), -800952 (**2**·MeOH) and –800953 (**2**·CD_3OD). These data can be obtained free of charge from The Cambridge Crystallographic Data Centre via www.ccdc.cam.ac.uk/data_request/cif.

Acknowledgments

This work has been supported financially by the Deutsche Forschungsgemeinschaft (WE 3546_4-1), the Fonds der Chemischen Industrie, the Center for Integrated Protein Science Munich (CIPSM), the University of Munich, the Interuniversity Attraction Pole VI (P6/17) INANOMAT "Advanced Complex Inorganic Materials by a Novel Bottom-up Nanochemistry Approach: Processing and Shaping", the Fonds National de la Recherche Scientifique – Fonds de la Recherche Fondamentale Collective, a Concerted Research Action of the "Communauté Française de Belgique" allotted by the Académie Universitaire Louvain and by the European Social Fund through Sectorial Operational Program Human Resources: PRiDE (No. POSDRU/89/1.5/S/57083).

[1] a) H. A. Goodwin, *Coord. Chem. Rev.* **1976**, *18*, 293; b) E. König, *Struct. Bonding (Berlin)* **1991**, *76*, 51; c) P. Gütlich, A. Hauser, H. Spiering, *Angew. Chem.* **1994**, *106*, 2109; *Angew. Chem. Int. Ed. Engl.* **1994**, *33*, 2024, and references cited therein; d) P. Gütlich, H. A. Goodwin (Eds.), "Spin Crossover in Transition Metal Compounds I–III" in *Topics in Current Chemistry*, Springer-Verlag, Berlin, **2004**; e) J. A. Real, A. B. Gaspar, M. C. Munoz, *Dalton Trans.* **2005**, 2062; f) K. Nakano, N. Suemura, K. Yoneda, S. Kawata, S. Kaizaki, *Dalton Trans.* **2005**, 740; g) O. Sato, J. Tao, Y.-Z. Zhang, *Angew. Chem.* **2007**, *119*, 2200; *Angew. Chem. Int. Ed.* **2007**, *46*, 2152; h) J. A. Kitchen, S. Brooker, *Coord. Chem. Rev.* **2008**, *252*, 2072; i) K. S. Murray, *Eur. J. Inorg. Chem.* **2008**, 3101; j) M. A. Halcrow, *Coord. Chem. Rev.* **2009**, 2059; k) S. Brooker, J. A. Kitchen, *Dalton Trans.* **2009**, 7331; l) C. J. Kepert, *Aust. J. Chem.* **2009**, *62*, 1079; m) K. S. Murray, *Aust. J. Chem.* **2009**, *62*, 1081; n) A. B. Koudriavtsev, W. Linert, *J. Struct. Chem.* **2010**, *51*, 335.

[2] a) O. Kahn, C. Jay Martinez, *Science* **1998**, *279*, 44; b) O. Kahn, C. Jay Martinez, J. Kröber, R. Claude, F. Grolière, EP0666561, **1995**; c) J.-F. Létard, O. Nguyen, N. Daro, FR0512476, **2005**; d) J.-F. Létard, P. Guionneau, L. Goux-Capes, *Topics in Current Chemistry* (Ed.: P. Gütlich, H. A. Goodwin), Springer, Wien, **2004**, 221 (235 pp.); e) A. Galet, A. B. Gaspar, M. C. Muñoz, G. V. Bukin, G. Levchenko, J. A. Real, *Adv. Mater.* **2005**, *17*, 2949.

[3] Y. Garcia, V. Ksenofontov, P. Gütlich, *Hyperfine Interact.* **2002**, *139/140*, 543.

[4] Y. Garcia, V. Ksenofontov, S. Mentior, M. M. Dîrtu, C. Gieck, A. Bhatthacharjee, P. Gütlich, *Chem. Eur. J.* **2008**, *14*, 3745.

[5] a) M. Seredyuk, A. B. Gaspar, V. Ksenofontov, Y. Galyametdinov, M. Verdaguer, F. Villain, P. Gütlich, *Inorg. Chem.* **2008**, *47*, 10232; b) M. Seredyuk, A. B. Gaspar, V. Ksenofontov, Y. Galyametdinov, J. Kusz, P. Gütlich, *Adv. Funct. Mater.* **2008**, *18*, 2089; c) M. Seredyuk, A. B. Gaspar, V. Ksenofontov, Y. Galyametdinov, J. Kusz, P. Gütlich, *J. Am. Chem. Soc.* **2008**, *130*, 1431.

[6] a) J. A. Real, A. B. Gaspar, V. Niel, M. C. Muñoz, *Coord. Chem. Rev.* **2003**, *236*, 121; b) A. Bousseksou, G. Molnár, J. A. Real, K. Tanaka, *Coord. Chem. Rev.* **2007**, *251*, 1822.

[7] a) A. B. Gaspar, V. Ksenofontov, M. Seredyuk, P. Gütlich, *Coord. Chem. Rev.* **2005**, *249*, 2661; b) A. B. Gaspar, M. Seredyuk, P. Gütlich, *J. Mol. Struct.* **2009**, *924–926*, 9.

[8] a) I. Boldog, A. B. Gaspar, V. Martinez, P. Pardo-Ibanez, V. Ksenofontov, A. Bhattacharjee, P. Gütlich, J. A. Real, *Angew. Chem.* **2008**, *120*, 6533; *Angew. Chem. Int. Ed.* **2008**, *47*, 6433; b) S. Cobo, G. Molnar, J. A. Real, A. Bousseksou, *Angew. Chem.* **2006**, *118*, 5918; *Angew. Chem. Int. Ed.* **2006**, *45*, 5786; c) G. Molnár, S. Cobo, J. A. Real, F. Carcenac, E. Daran, C. Vieu, A. Bousseksou, *Adv. Mater.* **2007**, *19*, 2163.

[9] B. Weber, W. Bauer, J. Obel, *Angew. Chem.* **2008**, *120*, 10252; *Angew. Chem. Int. Ed.* **2008**, *47*, 10098–10101.

[10] A. P. Summerton, A. A. Diamantis, M. R. Snow, *Inorg. Chim. Acta* **1978**, *27*, 123.

[11] B. Weber, J. Obel, D. Henner-Vásquez, W. Bauer, *Eur. J. Inorg. Chem.* **2009**, 5527.

[12] a) A. Bhattacharjee, V. Ksenofontov, K. H. Sugiyarto, H. A. Goodwin, P. Gütlich, *Adv. Funct. Mater.* **2003**, *13*, 877; b) K. H. Sugiyarto, M. L. Scudder, D. C. Craig, H. A. Goodwin, *Aust. J. Chem.* **2000**, *53*, 755; c) A. Bhattacharjee, J. Kusz, M. Zubko, H. A. Goodwin, P. Gütlich, *J. Mol. Struct.* **2008**, *890*, 178.

[13] a) K. H. Sugiyarto, K. Weitzner, D. C. Craig, H. A. Goodwin, *Aust. J. Chem.* **1997**, *50*, 869; b) T. Buchen, P. Gütlich, K. H. Sugiyarto, H. A. Goodwin, *Chem. Eur. J.* **1996**, *2*, 1134.

[14] J. A. Real, A. B. Gaspar, V. Niel, M. C. Muñoz, *Coord. Chem. Rev.* **2003**, *236*, 121.

[15] N. Bréfuel, S. Imatomi, H. Torigoe, H. Hagiwara, S. Shova, J.-F. Meunier, S. Bonhommeau, J.-P. Tuchagues, N. Matsumoto, *Inorg. Chem.* **2006**, *45*, 8126.

[16] a) B. R. Müller, G. Leibeling, E.-G. Jäger, *Chem. Phys. Lett.* **2000**, *319*, 368; b) G. Leibeling, Ph.D. Thesis, University of Jena **2003**.

[17] C. Pike, A. Fernandez, *J. Appl. Phys.* **1999**, *85*, 6668.

[18] C. Enachescu, R. Tanasa, A. Stancu, E. Codjovi, J. Linares, F. Varret, *Phys. B* **2004**, *343*, 15.

[19] R. Tanasa, C. Enachescu, A. Stancu, J. Linares, E. Codjovi, F. Varret, J. G. Haasnoot, *Phys. Rev. B* **2005**, *71*, 014431.

[20] W. Vreugdenhil, J. H. Van Diemen, R. A. G. De Graaff, J. G. Haasnoot, J. Reedijk, A. M. Van Der Kraan, O. Kahn, J. Zarembowitch, *Polyhedron* **1990**, *9*, 2971.

[21] a) Y. Garcia, V. Niel, M. C. Muñoz, J. A. Real, *Top. Curr. Chem.* **2004**, *233*, 229; b) Y. Garcia, C. Gieck, S. Stauf, W. Tremel, P. Gütlich, 4th TMR TOSS-Meeting, Bordeaux, France, **2001**; c) S. Pillet, J. Hubsch, C. Lecomte, *Eur. Phys. J. B* **2004**, *38*, 541.

[22] M. M. Dîrtu, C. Neuhausen, A. D. Naik, A. Rotaru, L. Spinu, Y. Garcia, *Inorg. Chem.* **2010**, *49*, 5723.

[23] A. Rotaru, Ph.D. Thesis, Versailles, **2009**.

[24] B. Weber, E. Kaps, J. Weigand, C. Carbonera, J.-F. Létard, K. Achterhold, F. G. Parak, *Inorg. Chem.* **2008**, *47*, 487.

[25] a) B. Weber, *Coord. Chem. Rev.* **2009**, *253*, 2432; b) B. Weber, E.-G. Jäger, *Eur. J. Inorg. Chem.* **2009**, 465.

[26] a) B. Weber, E. Kaps, J. Obel, W. Bauer, *Z. Anorg. Allg. Chem.* **2008**, 1421; b) B. Weber, C. Carbonera, C. Desplanches, J.-F. Létard, *Eur. J. Inorg. Chem.* **2008**, 1589; c) B. Weber, E. Kaps, C. Desplanches, J.-F. Létard, K. Achterhold, F.-G. Parak, *Eur. J. Inorg. Chem.* **2008**, 4891; d) W. Bauer, B. Weber, *Inorg. Chim. Acta* **2009**, *362*, 2341; e) B. Weber, E. Kaps, *Heteroat. Chem.* **2005**, *16*, 391; f) B. Weber, E. Kaps, J. Obel, K. Achterhold, F. G. Parak, *Inorg. Chem.* **2008**, *47*, 10779; g) B. Weber, R. Tandon, D. Himsl, *Z. Anorg. Allg. Chem.* **2007**, *633*, 1159; h) B. Weber, E. S. Kaps, C. Desplanches, J.-F. Létard, *Eur. J. Inorg. Chem.* **2008**, 2963.

[27] K. Hosoya, T. Kitazawa, M. Takahashi, M. Takeda, J.-F. Meunier, G. Molnar, A. Bousseksou, *Phys. Chem. Chem. Phys.* **2003**, *5*, 1682.

[28] P. Gütlich, H. Köppen, H. G. Steinhäuser, *Chem. Phys. Lett.* **1980**, *74*, 475.

[29] N. Wiberg, *Holleman Wiberg – Lehrbuch der Anorganischen Chemie*, Walter de Gruyter, Berlin, **2007**.

[30] See for example: a) Y. Kikuta, T. Ishimoto, U. Nagashima, *Chem. Phys.* **2008**, *354*, 218; b) S. Singh, C. N. R. Rao, *Can. J. Chem.* **1966**, *44*, 2611.

[31] T. M. Pfaffeneder, S. Thallmair, W. Bauer, B. Weber, *New J. Chem.* **2010**, *35*, 691–700.

[32] a) K. H. Sugiyarto, H. A. Goodwin, *Aust. J. Chem.* **1988**, *41*, 1645; b) T. Buchen, P. Gütlich, H. A. Goodwin, *Inorg. Chem.* **1994**, *33*, 4573; c) K. H. Sugiyarto, D. C. Craig, A. D. Rae, H. A. Goodwin, *Aust. J. Chem.* **1994**, *47*, 869.

[33] Y. Garcia, S. J. Campbell, J. S. Lord, Y. Boland, V. Ksenofontov, P. Gütlich, *J. Phys. Chem. B* **2007**, *111*, 11111.

[34] a) J. Kröber, J. P. Audière, R. Claude, E. Codjovi, O. Kahn, J. G. Haasnoot, F. Grolière, C. Jay, A. Bousseksou, J. Linares, F. Varret, A. Gonthier-Vassal, *Chem. Mater.* **1994**, *6*, 1404; b) K. H. Sugiyarto, H. A. Goodwin, *Aust. J. Chem.* **1994**, *47*, 263.

[35] a) M. Sorai, S. Seki, *J. Phys. Soc. Jpn.* **1972**, *33*, 575; b) C. Chong, B. Berini, K. Boukheddaden, E. Codjovi, J. Linares, Y. Garcia, A. D. Naik, F. Varret, *Phys. Status Solidi A* **2010**, *207*, 1227.

[36] E.-G. Jäger, E. Häussler, M. Rudolph, M. Rost, *Z. Anorg. Allg. Chem.* **1985**, *525*, 67.

[37] B. Weber, R. Betz, W. Bauer, S. Schlamp, *Z. Anorg. Allg. Chem.* **2011**, *673*, 102.

[38] J.-P. Launay, M. Tourrel-Pagis, J.-F. Lipskier, V. Marvaud, C. Joachim, *Inorg. Chem.* **1991**, *30*, 1033.

[39] W. Eysel, K. H. Breuer, *Thermochim. Acta* **1982**, *57*, 317.

[40] A. Rotaru, M. M. Dîrtu, C. Enachescu, R. Tanasa, J. Linares, A. Stancu, Y. Garcia, *Polyhedron* **2009**, *28*, 2531.
[41] *SIR 97*, Campus Universitario Bari, **1997**; A. Altomare, M. C. Burla, G. M. Camalli, G. Cascarano, C. Giacovazzo, A. Guagliardi, A. G. G. Moliterni, G. Polidori, R. Spagna, *J. Appl. Crystallogr.* **1999**, *32*, 115.
[42] G. M. Sheldrick, *SHELXL 97*, University of Göttingen, Germany, **1993**.
[43] CCDC-723037 (**1**^{HT}D), CCDC-723038 (**1**^{LT}), CCDC-800952 (**2**·MeOH) and CCDC-800953 (**2**·CD_3OD) contains the supplementary crystallographic data for this paper. These data can be obtained free of charge from The Cambridge Crystallographic Data Centre via www.ccdc.cam.ac.uk/data_request/cif.
[44] C. K. Johnson, M. N. Burnett, "ORTEP-III", Oak-Ridge National Laboratory, Oak-Ridge **1996**; L. J. Farrugia, *J. Appl. Crystallogr.* **1997**, *30*, 565.

Received: April 1, 2011
Published Online: June 21, 2011

